Hydrodynamics of Taylor flow in small channels: a review

P Angeli* and **A Gavriilidis**
Department of Chemical Engineering, University College London, London, UK

The manuscript was received on 21 June 2007 and was accepted after revision for publication on 8 January 2008.

DOI: 10.1243/09544062JMES776

Abstract: The improved mass transfer characteristics of Taylor flow, make it an attractive flow pattern for carrying out gas–liquid operations in microchannels. Mass transfer characteristics are affected by the hydrodynamic properties of the flow such as thickness of the liquid film that surrounds the bubbles, bubble velocity, bubble and slug lengths, mixing, and flow circulation in the liquid slugs, and pressure drop. Experimental, theoretical, and modelling attempts to predict these properties are reviewed and relevant correlations are given. Most of these refer to capillaries but there are number of studies on square channels. In general, flow properties are well understood and predicted for fully formed Taylor bubbles in a developed flow and in clean systems, particularly in circular channels. However, the presence of impurities and their effect on interfacial tension cannot be fully accounted for. In addition, there is still uncertainty on the size of bubbles and slugs that form under certain operating and inlet conditions, while there is little information for channels with non-circular cross-sections.

Keywords: gas–liquid flow, Taylor flow, film thickness, bubble length, slug length, microchannels

1 INTRODUCTION

With the advances in microfabrication techniques, microstructured reactors, which have channels or geometric features in the order of microns to hundreds of microns, have become widely available. These reactors extend the range of capabilities of conventional reactors especially in terms of enhanced mass and heat transfer, which is simply a result of the large surface-to-volume ratio they offer. Initially used for single phase systems, their applications have now been extended to multiphase systems. In multiphase applications the distribution of phases in the channel (or the flow patterns that form) affects heat/mass transfer characteristics. The dominance of surface tension forces in small channels results in many cases in patterns different to those found in large scale systems. For example, stratified gas–liquid flow is rarely observed in small channels. In general, at low gas flowrates bubbles appear within a continuous liquid phase. As the gas flowrate increases Taylor flow forms, which consists of elongated bubbles with equivalent spherical diameter usually many times that of the channel diameter, separated by liquid slugs (Fig. 1(a)). With further increase in gas flowrate annular flow appears with the liquid forming an annulus wetting the wall. At high gas and liquid flowrates churn flow occurs where there is a liquid film at the wall and gas flow in the centre within which frothy slugs appear frequently.

As the channel dimensions reduce, Taylor and annular flows dominate while patterns specific to small channels appear (such as ring, liquid lump, yakitori, and rivulet) which can be considered as variations of the Taylor and annular flow regimes. A recent review on flow patterns during gas–liquid flow in microchannels was given by Ghiaasiaan and Abdel-Khalik [**1**].

It is noted here that channels are generally regarded small when surface tension forces dominate gravitational forces. A measure of the relative value of the two forces is given by the Eötvös or Bond number (both names are used invariably in the literature)

$$Bo \text{ or } E\ddot{o} = \frac{(\rho_g - \rho_l) g d^2}{\sigma} \tag{1}$$

where ρ_g and ρ_l are the gas and liquid densities, respectively, g the gravitational acceleration, d the tube diameter, and σ the surface tension. Investigators have suggested different values of the Bo or $E\ddot{o}$ below which channels can be considered small ranging from

*Corresponding author: Department of Chemical Engineering, University College London, Torrington Place, London WC1E 7JE, UK. email: p.angeli@ucl.ac.uk

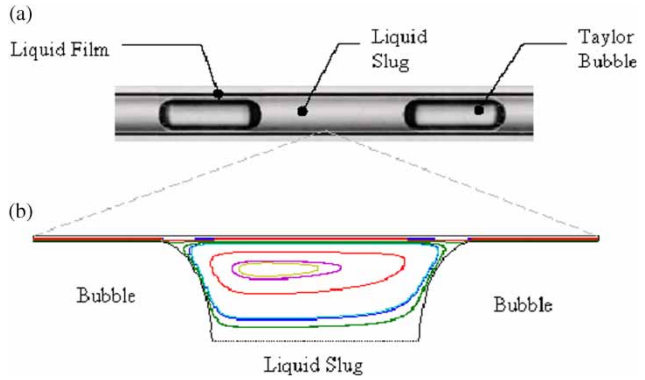

Fig. 1 Gas–liquid Taylor flow streamlines in the liquid slug

0.88 to $(2\pi)^2$ [**2**, **3**]. Bretherton [**4**] observed that a Taylor bubble does not rise spontaneously in a water-filled vertical capillary under the effect of gravity for $E\ddot{o}$ <3.37, and this value can also be used to define small channels. By combining data from various investigators in a graph of Fr ($Fr = U_b/(gd)^{1/2}$, U_b is the bubble velocity) versus $E\ddot{o}$, it was shown that bubble terminal velocity (rise velocity in a stagnant liquid) becomes 0 for $E\ddot{o} < 4$ [**5**]. For an air–water system the above criteria give channel sizes between 2.6 and 17 mm for transition to small (or micro) channel flow. Generally, however, it is accepted that transition to surface tension dominated flows, which signify small channels, occurs for channel diameters between 1 and 2 mm [**6**, **7**].

In Taylor flow (also referred to as bubble train, slug, segmented, plug, elongated bubble, or intermittent flow), the bubbles adopt a characteristic capsular shape and can either completely or nearly completely fill the channel cross-section where at most a thin liquid film separates them from the channel wall. One of the first applications of Taylor bubbles was in flow measurement where bubbles acted as tracers in capillaries filled with liquid to determine the liquid velocity. Later, however, it was recognized that the presence of the film that separates the bubble from the wall also means that the bubble velocity is not equal to the liquid one. The presence of bubbles in front and at the back of the slugs, modifies the flow field in the liquid slug compared with single-phase flow and toroidal vortices extending the length of the slug can form (Fig. 1(b)). As a result of the modification of the flow field in the slugs, Taylor flow offers many advantages for carrying out reactions compared with other patterns and to single-phase laminar flow [**8**]. The separation of the bulk liquid by the bubbles significantly reduces liquid axial mixing [**9**, **10**]. The film surrounding the bubbles is the only means of communication between two successive slugs and in the majority of cases its thickness is only a very small percentage of the tube diameter. The recirculation within the liquid slugs improves heat and mass transfer from liquid to wall and interfacial mass transfer from gas to liquid [**11**]. The combination of good radial mass transfer and low axial mass transfer in the liquid makes Taylor flow suitable for two-phase applications that involve mass transfer or single-phase liquid applications which suffer from large back-mixing. The former case includes fast multiphase reactions that can be mass transfer limited. In fact, a lot of information on Taylor flow originates from the investigations of the monolith froth reactor where the two fluid phases are introduced into the reactor as froth flow and pass through the catalyst coated channels in a Taylor flow pattern. The performance of tubes with absorbing walls for liquid chromatography and of tubular dialysers can be improved when they are operated in Taylor compared with single phase flow. Even microfiltration efficiencies have been found to improve when Taylor bubbles are used in the liquid medium, attributed to the wall shear stress increase and pulsations caused by the alternating passage of slugs and bubbles [**12**]. The low axial mixing properties of Taylor flow have been used in automated analysers, where successive samples in the feed line should not interact. The same concept applies to high throughput screening where Taylor bubbles facilitate the sequential passage of different reactants/samples through a microchannel reactor/analyser. The enhanced heat and mass transfer rates possible in microchannels would enable a kinetically controlled operating regime to be established that allows evaluation of reaction kinetics.

Knowledge of hydrodynamic characteristics during Taylor flow is necessary for understanding the behaviour and improving the performance of microchemical systems that operate in this regime. Properties such as thickness of film that surrounds the bubbles, bubble shape and velocity, bubble and slug length, flow patterns in the liquid slug, and pressure drop, have been studied by a number of investigators particularly for capillaries. In the current paper, the key research findings are presented for circular channels, while the still limited information for non-circular channels is also discussed.

2 CIRCULAR CHANNELS

2.1 Film thickness

The flow of a long bubble in a capillary is a classical problem in fluid mechanics. Bubbles had often been used in capillaries filled with liquid as tracers to determine the velocity of the liquid. However, Fairbrother and Stubbs [**13**] observed that a wetting film is deposited on the wall of a capillary when a wetting viscous liquid is displaced by a gas bubble.

Table 1 Experimentally obtained film thickness

Dimensionless film thickness, δ/r	Range of Ca	Measuring technique	Reference
$0.5\,Ca^{1/2}$ (2)	$5\times10^{-5}\leqslant Ca\leqslant 3\times10^{-1}$	Movement of indicator bubble/conductimetry	[**13–15**]
$\left(0.89-\dfrac{0.05}{U_g^{1/2}}\right)Ca^{1/2}$ (3)	$7\times10^{-6}\leqslant Ca\leqslant 2\times10^{-4}$	Conductimetric technique	[**16**]
U_g in cm/s			
$1.34\,Ca^{2/3}$ (4)	$10^{-3}\leqslant Ca\leqslant 10^{-2}$	Volumetry	[**4**]
$0.36[1-\exp(-3.08(Ca^{0.54}))]$ (5)	$9.5\times10^{-4}\leqslant Ca\leqslant 1.9$	Light absorption	[**17**]
$\dfrac{(1.34Ca^{2/3})}{1+2.5(1.34Ca^{2/3})}$ (6)	$10^{-3}\leqslant Ca\leqslant 1.4$	Video recording	[**18**]

Their experiments indicated that the film thickness was proportional to $Ca^{1/2}$ (where the capillary number, $Ca=\mu_l U_b/\sigma$ and μ_l is the liquid viscosity) for $7.5\times10^{-5}<Ca<0.014$ (see Table 1). In subsequent experimental work, this finding was confirmed and extended up to $Ca=10^{-1}$ [**14**]. In his pioneering analytical approach, Bretherton [**4**] assumed creeping flow in the liquid film and used lubrication theory for the region of the film between the end of the spherical bubble cap and the flat film behind it to calculate film thickness, pressure drop, and bubble shape. The Taylor bubble was taken as inviscid with spherical caps. From this analysis it was found that $\delta/r=1.34Ca^{2/3}$, where δ is the film thickness and r the capillary radius. This finding should be valid for low Ca. Surprisingly, however, experiments agreed better with the theory for Ca equal to 10^{-3}, while at lower Ca, where the theory should hold exactly, the film thickness was substantially larger than the theoretical values. Attempts to explain this discrepancy based on non-zero dispersed phase viscosity [**19**], intermolecular forces [**20**, **21**], and surface roughness [**15**] were not successful. On the other hand, the presence of surface-active contaminants that are absorbed at the interface could affect film thickness. Surfactants would render the interface rigid. Considering a rigid interface (no-slip condition) in the transition region between the bubble cap and the film, Bretherton [**4**] showed that the film thickness would increase by a factor of $2^{2/3}$. By assuming a rigid bubble interface which is stationary in the laboratory frame, the film thickness was found to increase by a maximum factor of $4^{2/3}$, which bounds most of the available data [**22**]. Ratulowski and Chang [**23**] argued that surface contamination can be correctly assessed only if the variation of the surface tension along the interface is considered. Improving on previous attempts, they developed a model that included both surfactant transport at the interface and in the bulk liquid and showed that an increase in film thickness occurs if surfactant transport in the bulk is mass transfer limited and a concentration gradient exists. Concentration gradients in the bulk will cause the surfactant concentration at the interface to decrease from the bubble cap towards the film. The surface tension in the film is then larger than its value at the cap and a surface traction in the direction of the film is created, which induces more liquid to flow into the film and increase its thickness. This is more significant at low Ca, because at high Ca horizontal flow by convection in the film overcomes the flow imposed by the surface traction.

For higher values of Ca ($Ca>5\times10^{-3}$) numerical studies are required to obtain bubble shape and film thickness. A number of numerical solutions to the problem of a moving bubble in a liquid medium have been suggested, which also validate Bretherton's approach at very low Ca. As the front profile and film thickness of a long Taylor bubble with sufficient separation between the bubbles can be approximated by that of an infinitely long bubble, many, particularly initial, studies considered semi-infinite bubbles. Also progressively higher Ca were investigated. Reinelt and Saffman [**24**] used a finite difference method to study a semi-infinite bubble for $10^{-4}<Ca<0.1$. Shen and Udell [**25**] used a finite element method with deformable grid to study a semi-infinite bubble for Ca up to 0.1. The work was extended with the application of a boundary element method to the study of the front and back of the bubble separately (two semi-infinite bubble analyses) for $10^{-2}<Ca<10$ and $10^{-2}<Ca<1.5$, respectively [**26**]. These simulations confirmed Bretherton's theory [**4**] for low Ca while for higher Ca the numerical results agreed with the correlation by Fairbrother and Stubbs [**13**].

The whole bubble was studied by Ratulowski and Chang [**27**] who used an arclength-angle formulation of a composite lubrication equation without assuming constant film thickness, to extend the analysis by Bretherton to higher Ca. The results on film thickness agreed well with Bretherton's theory for $Ca<0.01$. At higher Ca, though, larger film thickness was calculated than that predicted by Bretherton, which agreed with the results by Reinelt and Saffman [**24**] for Ca up to about 0.5. Finite bubbles with lengths larger than the channel width were shown to resemble infinitely long bubbles on film thickness and pressure drop.

The effect of inertia was first modelled by Edvisson and Irandoust [**28**] using finite elements where the bubble and the coordinate system velocity were matched. The effect of capillary, Reynolds, and Froude numbers were studied with *Ca* varying from 0.01 to 1, *Re* from 20 to 200, and *Fr* was either 0 (no gravitational effects) or 1. The Reynolds number was taken equal to $Re = \rho_l U_m d/\mu_l$, based on the two-phase mixture velocity, U_m, (equal to the sum of the gas and liquid superficial velocities) rather than the more commonly used bubble velocity. The simulations revealed that the film thickness also depended on *Fr* and *Re*. As *Re* increases the film thickness and the velocity difference between the phases also increase. *Fr* had an effect at higher *Ca* where with increasing *Fr* the film thickness and bubble velocity slightly decrease for downward flow but increase significantly for upward flow. With increasing *Ca* also the bubble shape at the back changed from convex to concave. At the higher *Re* studied ripples appeared at the back of the bubble, although the authors admitted that the solutions at these conditions may not have fully converged. Both amplitude and wavelength of these ripples go through a maximum with increasing *Ca*.

The effect of inertia was also investigated by Giavedoni and Saita who improved the approach and used adjustable meshes while updating the velocity boundary conditions in each iteration to keep the bubble stationary. The front [**29**] and back [**30**] of a Taylor bubble were analysed separately for $10^{-5} < Ca < 10, Re < 70$, and $10^{-3} < Ca < 1.5$, $Re < 70$, respectively. Because of the development of a constant film thickness, it is possible to study the front and rear parts of the bubble independently. Good agreement was found with Bretherton's theory for $Ca < 10^{-3}$. The influence of *Re* on film thickness was found to be slight but non-monotonic; with increasing *Re* film thickness initially decreased and then increased. However, for $Ca < 0.01$ inertial forces did not have an effect on film thickness. The bubble front tended to adopt the shape of an arc of a circle for decreasing *Ca*. Undulations appeared at the back of the bubble, which depended on both *Ca* and *Re* and at low *Ca* and *Re* agreed with Bretherton's theory. Larger Reynolds numbers appear to produce larger undulations. As inertial forces increased the amplitude of the undulations increased and the wavelength decreased. For $Ca > 0.5$ no undulations were observed. For all *Re* tested the back of the bubble was convex at first, became flat as *Ca* increased and then adopted a concave shape (as also shown by reference [**28**]), while with increasing *Re* the change from flat to concave shape appeared at lower *Ca* (Fig. 2). For $Ca < 10^{-3}$, close to the meniscus tip the interface is an almost perfect hemisphere. Taha and Cui [**12**] used a commercial computational fluid dynamics (CFD) software based on finite volumes and the volume of fluid (VOF) method to reproduce the

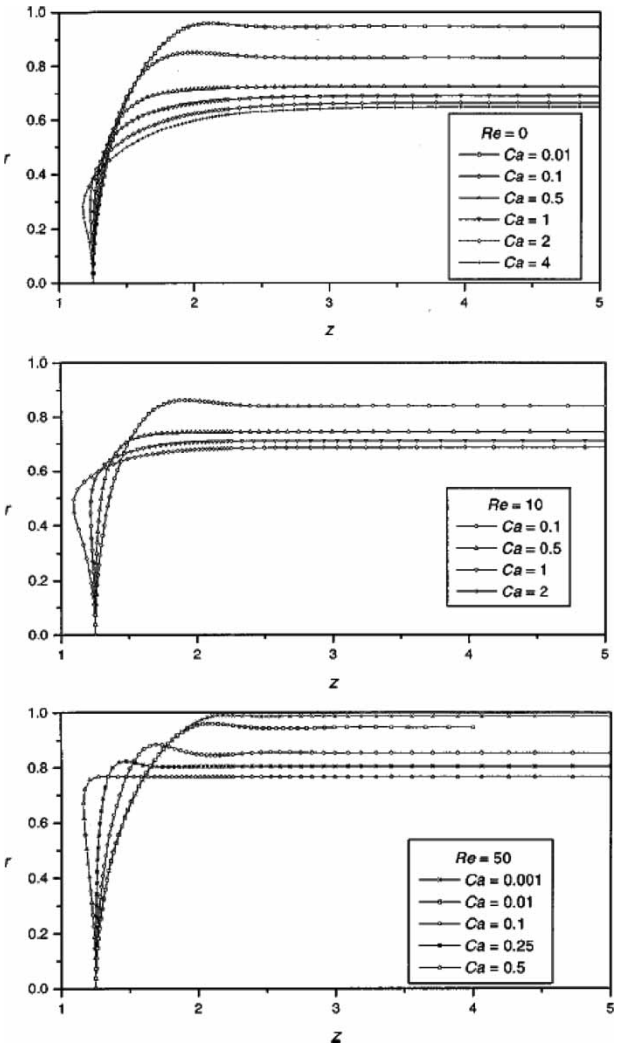

Fig. 2 Shape of the rear meniscus of a Taylor bubble for different *Ca* and increasing *Re* (from reference [**30**]). Larger *Ca* corresponds to thicker films

interface and for $Ca < 2.4$ found a similar effect of *Ca* on bubble shape. The transition region between the front of the bubble cap and the area of constant film thickness diminished with decreasing *Ca*.

Inertia effects were further studied by Heil [**31**] who used a similar technique to Giavedoni and Saita but in a two-dimensional channel and extended the region of *Re* up to 280 for $0.05 < Ca < 5$. His results confirmed the findings by Giavedoni and Saita [**29**] and showed that the film thickness continued to increase as a result of inertia for $Re > 70$ (Fig. 3). De Ryck [**32**] extended Bretherton's theory to include inertial effects in circular geometries based on a regular perturbation method. *Re* up to 1000 were studied which confirmed the findings on film thickness of Giavedoni and Saita and Heil at lower *Re* and showed that at even higher *Re* the film thickness further increases.

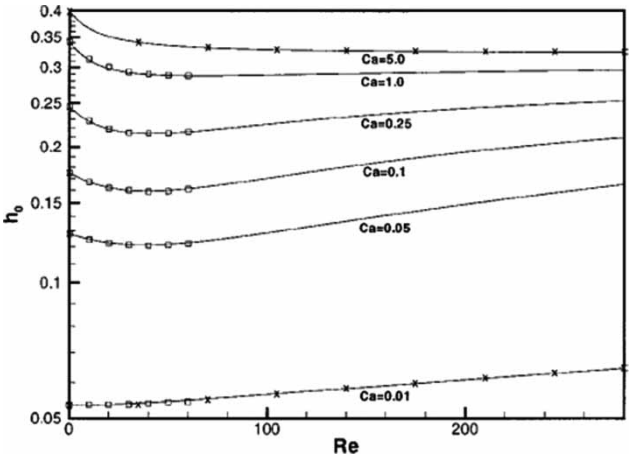

Fig. 3 Dimensionless film thickness, h_0, as a function of *Re* for increasing *Ca* (from reference [**31**])

To evaluate the film thickness Aussilous and Quéré [**18**] used scaling arguments in a semi-infinite bubble instead of numerical simulations. For the viscocapillary regime (where the film thickness depends only on *Ca*) a correlation was suggested that agreed well with Taylor's [**14**] data and at very small *Ca* with Bretherton's [**4**] model. After fitting it to experimental data the correlation took the form of equation (6) in Table 1. At $Ca > 10^{-3}$ inertial effects become important (viscoinertial regime) and the film thickens, deviating from Taylor's findings. The deviation starts to occur at a critical *Ca*, $Ca^* \propto \mu_l^2/\sigma\rho_l r$ and increases with increasing tube diameter. In this regime

$$\frac{\delta}{r} \propto \frac{Ca^{2/3}}{(1 + Ca^{2/3} - We)} \tag{7}$$

where $We = \rho_l U_b^2 (r - \delta)/\sigma$. In the above equation, the improvements over the Bretherton equation appear antagonistic; $Ca^{2/3}$ in the denominator favours convergence of the film thickness to a constant value while *We* (and inertia) increases it. At even higher velocities (and *We*) where surface tension forces become negligible the thickness of the film can be limited by the thickness of the viscous boundary layer that develops in the liquid as it moves.

Thulasidas *et al.* [**33**] developed a hydrodynamic analytical model for a unit cell (i.e. a bubble and a slug) that required as input the superficial gas and liquid velocities and a correlation between bubble diameter/film thickness and *Ca*. In the range of parameter values considered, gravity could not be neglected. The model predicted reasonably well the experimental flow parameters obtained during bubble train flow (more than one bubbles present in the tube) such as bubble velocity, gas volume fraction, and the ratio of bubble to unit cell length. The experimental bubble diameters agreed with Taylor's [**14**] data especially in horizontal flow. The film thickness was almost the same in horizontal and downward flows but twice as much in upward flow, similar to the predictions by [**28**].

A number of investigators have obtained experimentally correlations for the film thickness, which are given in Table 1. In summary, equation (6) [**18**] can be used for low *Ca*. This tends to the Bretherton analytical solution for very low *Ca* (equation (4)) and agrees with that by Taylor [**14**] and Fairbrother and Stubbs [**13**] (equation (2)) for the rest of the *Ca* range of its validity. Equations (3) [**16**] and (5) [**17**] give similar results, which are only slightly higher than those predicted by equation (6). When inertia becomes important the experimental data by Aussilous and Quéré [**18**] represented by equation (7) and the numerical results by Giavedoni and Saita [**29**], Heil [**31**], and de Ryck [**32**] can be used to calculate film thickness.

2.2 Bubble velocity

To evaluate bubble velocity in Taylor flow the drift flux model can be used [**34**]

$$U_b = CU_{ls} + U_o \tag{8}$$

where *C* is an experimentally determined coefficient, U_{ls} the average slug velocity, and U_o is the bubble rise velocity in a stagnant liquid whose value depends on the tube inclination. In a vertical tube, it is the bubble terminal velocity. For small capillaries the bubble rise velocity is very small or zero because of the surface tension effects (see also definition of small channels in section 1) and usually negligible compared with the liquid slug velocity. In this case the above equation reduces to

$$\frac{U_b}{U_{ls}} = C \tag{9}$$

The bubble motion is often characterized by a dimensionless number, *m*, that gives the relative velocity between the bubble and the liquid

$$m = \frac{U_b - U_{ls}}{U_b} \tag{10}$$

From their experimental results, Fairbrother and Stubbs [**13**] suggested the following correlation for *m*

$$m = 1.0\, Ca^{1/2} \tag{11}$$

As with the film thickness, the correlation was valid for $7.5 \times 10^{-5} < Ca < 0.014$. Its validity was extended for *Ca* up to 10^{-1} [**14**]. For large *Ca*, *m* acquired a constant value of 0.58, while theoretically it was found to be equal to 0.6 [**35**]. This was confirmed by the numerical simulations of Giavedoni and Saita [**29**] who found $m = 0.592$ for $Ca = 10$. From experimental data

in $7 \times 10^{-6} < Ca < 2 \times 10^{-4}$ and capillaries of various inclinations, Marchessault and Mason [**16**] derived the following equation

$$m = \left(\frac{\mu_l}{\sigma}\right)^{1/2} \left[-0.10 + 1.78\sqrt{U_b}\right] \tag{12}$$

Bretherton's [**4**] analytical approach at low *Ca* resulted in the following expression

$$m = 1.29(3\,Ca)^{2/3} \tag{13}$$

For vertical tubes, Bretherton introduced a correction to the above equation using a factor of $(1 \pm (1/6)E\ddot{o})$ for upward and downward flow, respectively. Thulasidas *et al.* [**33**] compared their own experimental data and all other data available in the literature on relative bubble velocity, *m*, against the correlations by Bretherton [**4**] and Marchessault and Mason [**16**], covering a large *Ca* range ($10^{-6} < Ca < 10$). There was considerable scatter of the experimental data at the lower *Ca*, while Bretherton's correlation was found to underpredict all data. The results did, however, confirm that *m* reached a limiting value of 0.58 at large *Ca*.

Laborie *et al.* [**36**] from experiments in bubble train flow ($55 < Re < 2000, 0.13 < E\ddot{o} < 5, 1.5 \times 10^{-3} < Ca < 10^{-1}$) found that the bubble velocity can be described by

$$U_b = C_o U_m \tag{14}$$

where C_o is a function of $E\ddot{o}$. For $E\ddot{o} \to 0$, C_o tends to a single value of 1.7, but for $E\ddot{o} > 0$, $C_o = aE\ddot{o}^b$. The values of *a* and *b* were found to depend on the fluid property number, N_f ($N_f = g\mu_l^4/\sigma^3\rho_l$) as given in Table 2.

By correlating all their experimental data in both circular and square capillaries, Liu *et al.* [**37**] derived the following correlation of bubble velocity in bubble train flow

$$\frac{U_b}{U_m} = \frac{1}{1 - 0.61\,Ca_m^{0.33}} \tag{15}$$

which is valid for $2 \times 10^{-4} < Ca_m = \mu_l U_m/\sigma < 0.39$.

Table 2 Dependence of parameters *a* and *b* in $C_o = aE\ddot{o}^b$ on the fluid property number, N_f (from reference [**36**])

N_f	*a*	*b*
4.7×10^{-11}	0.95	−0.10
9×10^{-11}	0.86	−0.09
3.2×10^{-10}	1.17	−0.11
6.9×10^{-8}	1.08	−0.07

Akbar and Ghiaasiaan [**38**] found that this correlation predicted well their data on bubble velocity (for $0.005 < Ca < 0.05$) obtained from numerical simulations of Taylor bubbles in a 1 mm capillary. They also showed that this equation predicted most of the data by Liu *et al.* [**37**] well and slightly underpredicted the data by Laborie *et al.* [**36**].

2.3 Bubble and slug lengths

Transport phenomena in Taylor flow (such as pressure drop and mass transfer rates) depend on the bubble and slug sizes. The analysis developed by Thulasidas *et al.* [**33**] allows the length ratio of bubble to unit cell to be calculated when the superficial gas and liquid velocities are known. The absolute lengths, however, will depend on the gas–liquid interaction at the inlet.

Laborie *et al.* [**36**] studied experimentally Taylor flow in capillaries with 1–4 mm diameter for $55 < Re < 2000, 0.13 < E\ddot{o} < 5, 1.5 \times 10^{-3} < Ca < 10^{-1}$. Air was injected at the bottom of the test section through a porous membrane. Well established Taylor flow was found only for the small capillaries, while in the larger ones bubble coalescence was seen all along the pipe and liquid slugs contained small bubbles. From the fluid properties investigated surface tension seemed to affect bubble but not liquid slug length, while an increase in liquid viscosity led to a decrease of both bubble and slug lengths. Bubble length was also found to decrease when capillary size increased. An increase in gas superficial velocity increased bubble but decreased slug length, while liquid superficial velocity did not have an effect. The experimental bubble, L_B, and slug, L_S, lengths were correlated to Reynolds and Eötvos numbers as shown below

$$\frac{L_B}{d} = 0.0878\frac{Re_{U_b}^{0.63}}{E\ddot{o}^{1.26}}, \quad Re_{U_b} = \frac{\rho_l U_b d}{\mu_l} \tag{16}$$

$$\frac{L_S}{d} = 3451\left(\frac{1}{Re_{U_g}E\ddot{o}}\right)^{1.27}, \quad Re_{U_g} = \frac{\rho_l U_g d}{\mu_l} \tag{17}$$

where U_g is the gas superficial velocity, $0.1 < U_g < 0.74$ m/s.

Bubble frequency was also investigated and was found to increase with increasing capillary size and gas and liquid superficial velocities. Viscosity also seemed to affect bubble frequency but not surface tension.

Kreutzer [**39**] and Kreutzer *et al.* [**40**] suggested that slug length could be calculated from the experimentally measured friction factors. The approach was validated for slug lengths formed in monolith reactors (see section 3.4 below). Liu *et al.* [**37**] used the dependence of mass transfer coefficient on slug length to derive an empirical correlation for the latter based on experimental data in circular and square channels, in which the gas and the liquid were introduced at the

opposite sides of a T-junction

$$\frac{U_{\mathrm{m}}}{\sqrt{L_{\mathrm{S}}}} = 0.088\, Re_{\mathrm{g}}^{0.72} Re_{\mathrm{l}}^{0.19} \tag{18}$$

where $Re_{\mathrm{g}} = \rho_{\mathrm{g}} U_{\mathrm{g}} d/\mu_{\mathrm{g}}$, $Re_{\mathrm{l}} = \rho_{\mathrm{l}} U_{\mathrm{l}} d/\mu_{\mathrm{l}}$, and U_{g}, U_{l} are the gas and liquid superficial velocities.

Acceptable agreement was found between the predictions of this equation and most of their experimental data obtained in capillaries with diameters ranging from 0.9 to 3 mm. Discrepancies were found however, when compared with other literature correlations. Equation (17) gave a large scatter while an equation suggested by Kreutzer [**39**] based on experimental data from monoliths (it is given below as equation (30). largely underestimated the experimental data. The different configuration of the gas–liquid feed systems in these works was considered to contribute to the discrepancies.

Akbar and Ghiaasiaan [**38**] conducted CFD axisymmetric simulations to model a unit cell (one bubble and two half liquid slugs) using periodic boundary conditions at the cell inlet and outlet for a capillary of 1 mm diameter. In order to better predict their numerical results as well as those by previous investigators [**36**, **37**] they modified equation (18) to include a gas holdup term as shown below

$$\frac{U_{\mathrm{m}}^{-0.33}}{\sqrt{L_{\mathrm{S}}}} = 142.6 \varepsilon_{\mathrm{g}}^{0.56} \left(\frac{d}{L_{\mathrm{UC}}}\right)^{0.42} Re_{\mathrm{g}}^{-0.252} \tag{19}$$

where L_{UC} is the unit cell length.

Extensive numerical simulations on formation and channel flow of Taylor bubbles with the same CFD software were conducted by Qian and Lawal [**41**] for gas and liquid superficial velocities from 0.01 to 0.25 m/s in a 1 mm capillary for gas holdup $0.09 < \varepsilon_g < 0.91$, $15 < Re = \rho_{\mathrm{l}} U_{\mathrm{b}} d/\mu_{\mathrm{l}} < 1500$, $0.000\,278 < Ca < 0.01$. Simulations were mainly conducted for a two-dimensional geometry which, however, were found to agree well with three-dimensional ones in a circular geometry. Recognizing the importance of the inlet configuration on bubble and slug lengths, the two fluids were either brought separately into the main channel through a T-junction or they were premixed. Different results were obtained depending on the degree of premixing; the better the inlet premixing the shorter the bubble or slug length. Also the T-inlet orientation and the size of the inlet channels were found to affect lengths. In general, small mixing zones at the inlet favoured short bubbles and slugs. For given superficial gas and liquid velocities, a distribution of bubble sizes was found in the channel and this non-uniformity became more pronounced at increased velocities, although no coalescence was observed. Channel size and gas and liquid superficial velocities affected lengths, while surface tension had a slight effect, as was also found by Laborie *et al.* [**36**] and liquid viscosity had almost no influence. Their 148 sets of data were correlated within 10 per cent by the following equation of unit cell length

$$\frac{L_{\mathrm{B}} + L_{\mathrm{S}}}{d} = 1.637 \varepsilon_{\mathrm{g}}^{-0.893} (1 - \varepsilon_{\mathrm{g}})^{-1.05} Re^{-0.075} Ca^{-0.0687} \tag{20}$$

The Reynolds number is based on the bubble velocity which, for the cases studied, is approximately equal to the mixture velocity. Bubble and slug lengths can be obtained by multiplying the above equation with the respective phase volume fraction. The correlation showed that the bubble and slug lengths are mainly determined by the phase holdup while the Reynolds and capillary numbers have only a slight effect.

The effect of inlet configuration on bubble and slug size was demonstrated by Amador *et al.* [**42**]. T- and Y-junctions with different inlet channel dimensions and fluid joining angles were used as well as a co-flow configuration with the gas in the middle and the liquid in the annulus around it. Three main bubble formation mechanisms were identified. One of them, which involves bubble lift-off, neck formation between the bubble and the nozzle and finally neck break up and bubble detachment, resembles the mechanism of bubble formation from an orifice in an infinite liquid medium and was modelled analytically [**43**]. Bubble pairing was also observed at the inlet and when small non-Taylor bubbles formed, there was bubble coalescence in the main channel. Bubble length was found to depend mainly on the ratio of gas to liquid superficial velocities. The size of the gas inlet affected bubble length but not that of the liquid inlet. Furthermore, the angle that the two fluids joined had only a small effect on bubble size.

2.4 Flow patterns in liquid slug

Qualitative sketches of the flow streamlines in the liquid slug ahead of the bubble were proposed as early as 1961 [**14**] (Fig. 4). At high *Ca*, for $m > 0.5$, complete bypass flow was suggested with a single stagnation point at the bubble front. At low *Ca*, for $m < 0.5$ two possible reversal flow patterns were envisaged, one featuring a stagnation ring around the bubble cap (Fig. 4(b)) and the other featuring a single stagnation point at the bubble cap tip and a second one inside the liquid slug (Fig. 4(c)). Patterns (a) and (b) have been confirmed experimentally [**35**] and numerically [**26**, **44**]. Edvinsson and Irandoust [**28**] only reported pattern (b) probably because of the small values of *Ca* used.

The numerical study by Giavedoni and Saita [**29**] of the front of the bubble produced all three patterns

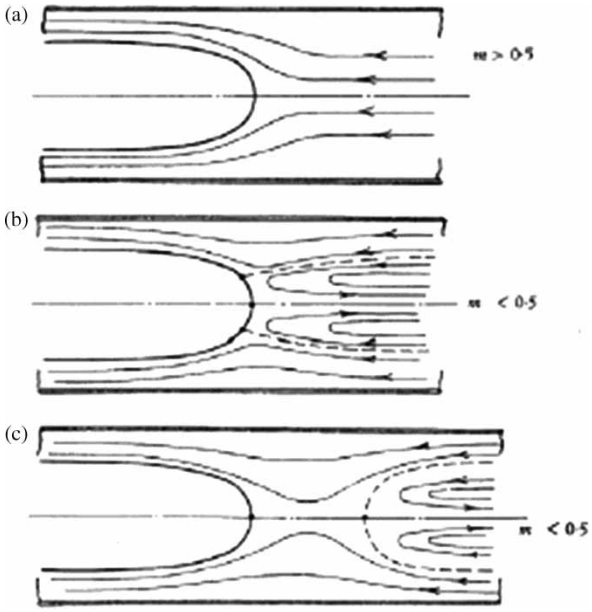

Fig. 4 Streamlines in the liquid slug in front of the Taylor bubble (from reference [**14**])

confirming Taylor's speculations. For no inertia and high *Ca*, bypass of the liquid and a single stagnation point on the bubble tip was observed. As *Ca* decreased, there was a transition and vortices started to appear at $Ca = 0.69$, as suggested by pattern (c). A stagnation ring was finally developed at $Ca = 0.60$ (pattern (b)). The small range of *Ca*, $0.60 < Ca < 0.69$ where pattern (c) appeared would explain why it has not been observed experimentally. At the back of the bubble it was shown that the flow can be divided into a zone of high velocities – external flow – (see Fig. 5(a)) and a zone of low velocities – internal flow – where the recirculation happens (shown as inserts in Fig. 5) [**30**]. As *Ca* increases from 0.60 to 0.70 the external flow remains almost the same but there are significant changes in the internal flow. The internal vortex diminishes in size and breaks into two regions, a swirl and a recirculating flow separated by a stagnation point, whose sizes diminish with increasing *Ca* (Figs 5(b) to (e)).

When inertia is important, the numerical simulations of Heil [**31**] revealed a change of the flow field in pattern (b) (Fig. 4(b)) ahead of the bubble. The streamlines which are drawn open in Fig. 4(b), change to form a closed vortex (from $Re = 20$). A 'cat's eye' pattern of successive vortices was suggested, whose sizes decreased rapidly with distance from the bubble tip.

The analytical model developed by Thulasidas *et al.* [**33**], suitable for bubble train flow, showed that transition to complete bypass occurs in horizontal

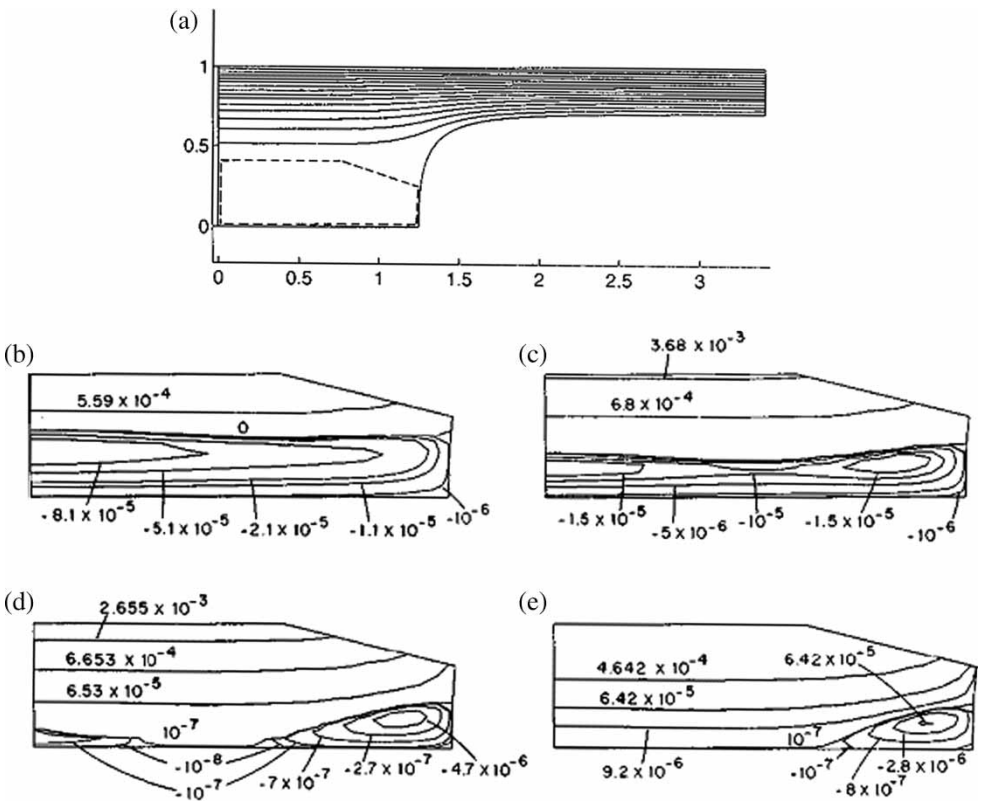

Fig. 5 Streamlines pertaining to both external (a) and internal ((b)–(e)) flow regions at the rear of the bubble for $Re = 0$, and for *Ca*: (a) 0.65; (b) 0.60; (c) 0.65; (d) 0.685; (e) 0.70 (from reference [**30**])

flow at $Ca = 0.7$, in upward flow at $Ca = 0.5$ and in downward flow at $Ca = 0.6$. Velocity profiles between two Taylor bubbles in vertical flow were studied experimentally [**45**] with particle image velocimetry (PIV) for $10^{-4} < Ca < 0.8$ and $10^{-4} < Re = \rho_l U_b d/\mu_l < 2$, $d = 2$ mm. Pattern (a) (Fig. 4(a)) was reported for $Ca > 0.47$ (bubble moves at the maximum liquid velocity at tube axis). The cat's eye pattern suggested by Heil [**31**] was not seen probably because of the small range of *Re* investigated. It is also possible that the interaction of the flow fields caused by the bubble caps enclosing a liquid slug would change the velocity profile compared with the semi-infinite analysis by Heil. In long slugs (larger than 1.5 times the channel diameter), parallel streamlines were found suggesting Poiseuille flow, while in short slugs this was not the case. Theoretically it was shown that for Poiseuille flow in pattern (b) (Fig. 4(b)) the radial position of the centre of the toroidal vortex, r^0, is given by

$$r^0 = \frac{r}{\sqrt{2}}\sqrt{2-\psi} \tag{21}$$

where $\psi = U_b/U_m$, while the radial position of the dividing streamline, r^1, that is the streamline which connects the stagnation points at the front and rear of the bubble and separates the circulating vortex from the liquid film attached to the wall is calculated from

$$r^1 = r\sqrt{2-\psi} \tag{22}$$

Both r^0 and r^1 become 0 at $\psi = 2.0$, (equivalent to $m = 0.5$) which is the point of complete bypass flow. Pattern (c) (Fig. 4(c)) was also obtained in the numerical simulations by Taha and Cui [**12**] of a Taylor bubble rising in a capillary for $Ca = 0.3$. Complete bypass was found for $Ca > 0.5$ which agrees with the results by Thulasidas *et al.* [**33**].

Also important is the speed at which the liquid in the vortex inside the slug moves as it will affect mixing. The dimensionless recirculation time, defined as the time required by the liquid slug to travel its own length during the time a particle in the recirculation vortex travels from one end of the slug to the other, was found from PIV measurements [**45**] to be approximately 2 for $Ca < 10^{-2}$. For larger *Ca*, the dimensionless recirculation time increases sharply and it becomes infinite for complete bypass flow.

2.5 Pressure drop

A variety of models have been suggested for calculating pressure drop during gas–liquid flow in large channels. A common one is the homogeneous model where the mixture of the two fluids is treated as one fluid with appropriately averaged properties that obey the usual equations of single-phase flow while there is no velocity difference between the two phases. Compared with other models, the homogeneous model was found by Triplett *et al.* [**6**] to predict better their experimental data on pressure drop during slug (equivalent to Taylor bubble) flow in circular and semi-semi-triangular cross-section channels with hydraulic diameters ranging from 1.1 to 1.5 mm. Liu *et al.* [**37**], however, suggested that the homogeneous model could only be used when the ratio of superficial gas to liquid velocity was less than 0.5, where the slip ratio *S* (defined as the ratio of actual gas to liquid velocity) is close to 1 according to their experimental data.

For shorter slugs the Laplace term in pressure drop, due to the effect of the bubbles on single phase liquid pressure drop, needs to be taken into account. The analysis by Bretherton [**4**] provided an expression of pressure drop, ΔP, across the bubble by using a matching method for the rear bubble transition region similar to the one used for the bubble front

$$\Delta P = 7.16(3\,Ca)^{2/3}\frac{\sigma}{d} \tag{23}$$

Kreutzer [**39**] calculated pressure drop over the bubble length using numerical simulations based on finite elements over a unit cell (a bubble and a slug). At low *Ca* the numerical results were slightly higher than Bretherton's predictions. His simulations indicated that pressure drop increases with increasing *Re* and decreasing *Ca*, while with increasing *Ca* the effect of inertia on pressure drop reduces. Heil [**31**] also found for a two-dimensional planar flow of a bubble front that the pressure required to drive the fluid increases with increasing *Re* and decreasing *Ca*. By subtracting the contribution of the liquid flow from the overall pressure drop in a unit cell, Kreutzer estimated the extra pressure drop caused by the presence of the bubble in the flow. It was found that this extra pressure drop was almost equal to the difference in interfacial pressure between the tips of the bubble at low *Re* while at high *Re*, the dramatic increase of pressure drop over the bubble interface was not observed for the entire unit cell. This was attributed to the fact that at low *Re* constant pressure lines, which originate from the bubble surface reach the wall, while at high *Re* there is a zone of high pressure close to the bubble tip, which does not reach the wall and therefore does not contribute to the overall pressure drop. Experimental data in a 2.3 mm capillary with water, decane, and tetradecane as liquid phases showed a strong dependence of pressure drop on slug length. Assuming that the pressure drop in a unit cell should consist of the pressure drop in the slug plus a term that accounts for the effects of the presence of the bubble in the flow (this includes liquid circulation effects and interfacial contributions), the following correlation was suggested for the friction factor, for $2 \times 10^{-3} < Ca < 4 \times 10^{-2}$ and *Re*

of the order of 100 [**46**]

$$f = \frac{16}{Re}\left[1 + \alpha_1 \frac{d}{L_S}\left(\frac{Re}{Ca}\right)^{1/3}\right] \tag{24}$$

where α_1 was found from the numerical simulations to be 0.07. However, a value of 0.17 fitted better the experimental data. The difference was attributed to the presence of impurities that could change the no-shear interfacial boundary condition to a no-slip one. From the above equation, for long slugs f approaches asymptotically $16/Re$, the Hagen–Poiseuille value for single phase flow in circular channels, while the effect of the extra term due to bubbles is important for $L_s/d < O(10^1)$. For low values of both Re and Ca (i.e. $Ca \ll 1$ and $Ca \times Re \ll 1$) Bretherton's equation (23) is valid which can be written in a form similar to equation (24)

$$f = \frac{16}{Re}\left[1 + \frac{d}{L_S}\frac{0.465}{Ca^{1/3}}\right] \tag{25}$$

Pressure drop in the channel can then be found from

$$\frac{\Delta P}{L} = \frac{2fU_m^2\rho_l}{d}\varepsilon_l \tag{26}$$

where L is the channel length and ε_l is the liquid phase volume fraction.

Based on experiments with three different liquids (water, ethanol, oil mixture) that had different viscosities and surface tensions, Liu *et al.* [**37**] suggested the following friction factor for $U_g/U_l > 0.5$, when the slip between the phases is large

$$F_E = \frac{C_f}{Re_E}S^{-0.5}[\exp(-0.02Re_E) + 0.07Re_E^{0.34}] \tag{27}$$

where C_f is the constant relating the Fanning friction factor to the laminar Reynolds number

$$Re_E = \frac{\rho_l U_E d}{\mu_l}$$

$$U_E = U_m + U_e = U_m + \left(\frac{d^2}{32\mu_l}\right)\rho_l g$$

U_E is the two-phase velocity and U_e is the gravity equivalent velocity. Pressure drop can then be found from

$$\frac{\Delta P}{L} = \frac{2F_E U_E^2 \rho_l}{d} \tag{28}$$

Taha and Cui [**12**] investigated the wall shear stresses along a Taylor bubble and within a slug by simulating with CFD a single Taylor bubble in an axisymmetric geometry. Shear stresses close to 0 were found along the liquid film while fluctuations and non-zero values were found at the front and back of the bubble, which were associated with the vortices in the slug and the waves at the bubble tail.

3 NON-CIRCULAR CHANNELS

Investigations on Taylor flow in non-circular channels originated from flows in porous materials as found for example in enhanced oil recovery. These flows are also highly relevant to microchannel applications where many of the macrofabrication techniques result in channels with non-circular cross-sections. However, Taylor flow in non-circular channels is much less studied that in circular ones while the available investigations cover almost exclusively square channels.

3.1 Bubble shape

Taylor flow in square channels was studied experimentally and theoretically by Kolb and Cerro [**47**–**49**]. Two bubble shapes were identified. At $Ca < 0.1$ the bubble is not axisymmetric and flattens out against the tube walls leaving liquid regions in the corners separated by thin flat films at the channel sides (Fig. 6(a)). At higher Ca an axisymmetric bubble is observed (Fig. 6(b)). At large Ca the bubble radius reaches an asymptotic minimum value, approximately equal to 0.68 times the channel width. The velocity profile in the film was calculated [**48**] and was then used in combination with the approach by Bretherton [**4**] to compute flow parameters in axisymmetric bubbles such as interface profiles, location of stagnation point and pressure gradient [**49**]. The calculations were carried out for intermediate to high Ca and $Eö$ where viscous, capillary, and gravity forces are important. Compared with experimental data, model predictions of bubble radius were particularly good for $Ca < 1.74$ with a slight overprediction for $Ca < 0.54$ and an underprediction for

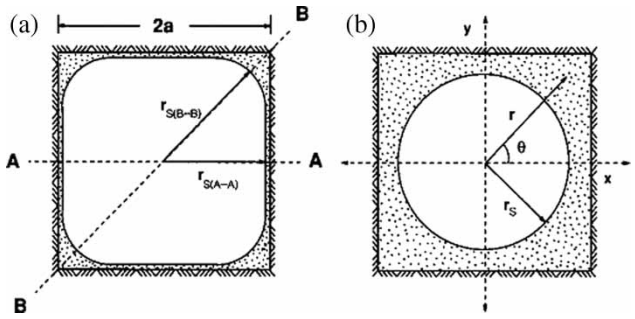

Fig. 6 Cross-section of a Taylor bubble inside a square channel: (a) non-axisymmetric bubble; (b) axisymmetric bubble (from reference [**48**])

$Ca > 0.54$. Thulasidas *et al.* [**33**] used the same theoretical approach as for circular capillaries to obtain flow parameters in square channels on the basis of superficial gas and liquid velocities. The model predictions compared reasonably well with experimental data in upward and downward flows. The transition between the two bubble shapes shown in Fig. 6 was identified to be at $Ca = 0.04$ (more precisely than by Kolb and Cerro [**47**]). From CFD simulations Taha and Cui [**50**] found that bubbles acquire spherical ends and are flat against the channel walls at low *Ca*, while at high *Ca* the shape at the back of the bubbles changes from convex to concave.

3.2 Film thickness

Film thickness in square capillaries both in the diagonal and axial directions has been measured experimentally [**33**, **47**] and also simulated [**51**]. The data were summarized in a graph by Kreutzer *et al.* [**52**] (Fig. 7) who also fitted the following correlation for bubble size in the diagonal direction

$$\frac{d_\mathrm{b}}{d_\mathrm{channel}} = 0.7 + 0.5\exp(-2.25Ca^{0.445}) \tag{29}$$

where d_b is the bubble diameter in the diagonal direction and d_channel is the square channel side length.

At low *Ca*, experimental film thickness in the axial and diagonal planes was found to be higher in upward than in downward flow [**33**]. Recently, Fries *et al.* [**53**] using confocal laser scanning microscopy found that for *Ca* around 0.002 the diagonal film thickness was close to the predictions of equation (29) while the axial one was close to the predictions of equation (7) [**18**]. Cubaud *et al.* [**54**] demonstrated experimentally that in square microchannels dry patches can appear on the side walls if the channel wall material is hydrophobic. These will cause loss of symmetry in a moving bubble in the direction of flow and lead to unsteady flow.

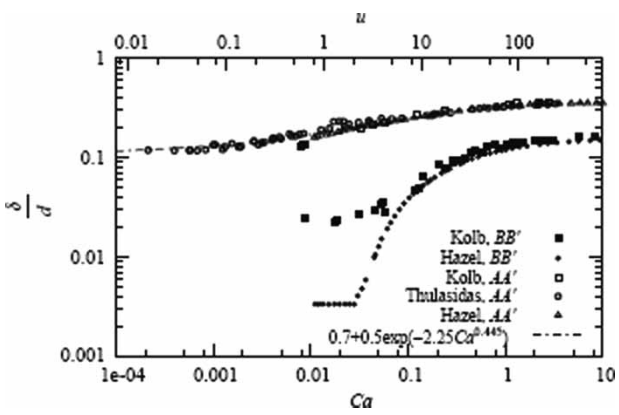

Fig. 7 Dimensionless film thickness versus *Ca* in square capillaries. On the top axis, the velocity of the bubble is plotted, assuming water-like properties $\mu_\mathrm{l} = 10^{-3}$ Pa s and $\sigma = 0.073$ N/m (from reference [**52**]). Directions AA′ and BB′ are equivalent to AA and BB in Fig. 6(a)

3.3 Bubble velocity

The dimensionless relative bubble velocity *m* (defined by equation (10)) was found by Thulasidas *et al.* [**33**] to approach asymptotically a limiting value of $m = 0.6$ at high *Ca*. At low *Ca*, differences between the upward and downward flow directions were observed; as *Ca* decreased *m* decreased for downward flow while for upward flow it showed a minimum at the point where the bubble diameter reaches a constant value, and then increased again. Equation (15) (in section 2.2) was developed including data from square channels as well [**37**]. Tsoligkas *et al.* [**55**] found that the drift flux model (equation (8) could describe well their experimental bubble velocities in downward flow, with the parameter C taking values between 1 and 1.3. Small but non-zero values were found for the rise velocity U_o, which indicate that gravity was still important in their 1.5 and 2 mm square channels with water or isopropanol/water as test liquids.

3.4 Bubble and slug lengths

Equation (18) [**37**] that was developed for both circular and square channels can be used to calculate liquid slug length. Based on the data by Heiszwolf *et al.* [**56**] in a 200 cells per square inch (31×10^4 cells per square metre) monolith reactor with a shower head as liquid distributor outside the monolith, Kreutzer [**39**] presented a correlation for slug length in square channels

$$\frac{L_\mathrm{S}}{d} = \frac{\varepsilon_\mathrm{l}}{-0.001\,41 - 1.556\varepsilon_\mathrm{l}^2 \ln(\varepsilon_\mathrm{l})} \tag{30}$$

More data on slug length were presented by Kreutzer *et al.* [**40**] from experiments in downflow monoliths using different types of distributors (nozzles with different sizes and shower heads). The slug length was also calculated from the experimentally measured friction factors using equation (24) where parameter 16, valid for circular channels, was substituted with the value of 14.2 for square channels. Good agreement was found with the direct slug length measurements apart from higher liquid hold ups. This methodology can be used for slug lengths less than ten times the pipe diameter, where friction factors are sensitive to variations in slug length.

The importance of gas and liquid flowrates on size of the formed bubble in a T-junction, demonstrated by many investigators for flows in circular channels (see section 2.3), was confirmed by the analysis of Garstecki

et al. [**57**] for non-circular channels. From order of magnitude calculations it was argued that at low *Ca*, as the bubble meniscus from the side channel advances into the main channel where the liquid flows and starts blocking it, the destabilizing effect of pressure that builds in the liquid upstream of the bubble is more significant than that of the shear stress of the liquid that flows in the available area around the bubble. The increased pressure 'squeezes' the neck that connects the forming gas bubble with its inlet channel which finally breaks. From simulations, the transition from 'squeezing' (pressure dominated) to 'dripping' (shear dominated) regime was found to be at $Ca = 10^{-2}$. In the 'squeezing' regime the following correlation was derived based on scaling arguments

$$\frac{L_B}{w} = 1 + \alpha \left(\frac{Q_g}{Q_l} \right) \tag{31}$$

where w is the main channel width, α is a fitting parameter of the order of 1, Q_l and Q_g are the liquid and gas flowrates, respectively. The correlation is valid at low *Ca*, for main channel width greater than its height and gas inlet width at least half that of the main channel. For $a = 1$, this equation also predicts Taylor bubble length obtained in mixing sections of cross geometry with square channels [**58**] and of co-flow geometry [**59**].

3.5 Flow patterns in liquid slug

Experimentally Kolb and Cerro [**47**] found transition to complete bypass in downward flow of an air bubble in square channels at $Ca = 0.6$. Using lubrication theory in a similar way to Bretherton [**4**], Kolb and Cerro [**49**] showed that for a bubble moving downwards in a stagnant liquid, complete bypass occurs at $Ca = 0.54$, where bubble velocity equals the maximum liquid velocity at the tube centre-line and the stagnation pressure is 0. For smaller *Ca* the bubble is faster than the average but slower than the maximum liquid velocity, which results in a stagnation ring on the bubble cap. Outside this ring, liquids flow past the bubble while inside the liquid recirculates. Thulasidas *et al.* [**33**] showed theoretically that complete flow bypass occurred at $Ca = 0.5$ for upward and at $Ca = 0.57$ for downward flow. Velocity profiles in the slugs were measured with PIV for upward [**45**] and for downward flow [**55**]. It was found that for upward flow the centre of the circulating vortex was closer to the tube wall than in downward flow. In addition, the dimensionless recirculation time (for definition see section 2.4) in the slug was found to be about 3 in upward flow, which was almost 3 to 4 times faster than in downward flow [**55**]. It was also found that the velocity profile in short slugs ($L_s <$ channel width) is much flatter compared with long slugs where it becomes parabolic [**55**].

3.6 Pressure drop

Kreutzer *et al.* [**40**] suggested that equation (24) could also be used for square channels if the limiting value for long slugs, 16, is substituted by that for square channels, 14.2. The empirically derived equation (21) can be used to calculate pressure drop in square channels [**37**]. Using CFD modelling Taha and Cui [**50**] calculated wall shear stresses, which for the sidewalls were found to fluctuate at the ends of the bubble in both upward and downward directions and to be almost zero within the liquid film. The wall shear stresses at the channel corners though were different for the two flow directions.

4 CONCLUSIONS

The hydrodynamic characteristics of Taylor bubbles flowing in small channels have been reviewed. Experimental, theoretical, and modelling attempts to understand and predict thickness of the liquid film that surrounds the bubbles, bubble velocity, bubble and slug lengths, mixing and flow circulation in the liquid slugs, as well as pressure drop during Taylor flow were presented for circular cross section channels, while the limited work on square channels was also discussed. These hydrodynamic properties appear to be well understood and predicted for fully formed Taylor bubbles in clean systems for developed flow in circular channels. However, the presence of impurities and uncertainties on the values of surface tension gradients at the gas–liquid interface render any theoretical analysis and modelling attempts more difficult and result in discrepancies between theoretical predictions or numerical simulations and experimental data. These can only be aggravated in systems where mass transfer and reactions occur and as a result concentrations vary with time. In addition, there is still uncertainty on the size of bubbles and slugs that form under certain operating and inlet conditions. Clearly more information and predictive models are needed for the hydrodynamic parameters in channels with non-square cross-sections while wall wetting and inlet configuration effects need to be further studied.

REFERENCES

1 **Ghiaasiaan, S. M.** and **Abdel-Khalik, S. I.** Two-phase flow in microchannels. *Adv. Heat Transf.*, 2001, **34**, 145–254.
2 **Brauner, N.** and **Moalem-Maron, D.** Identification of the range of "small diameters" conduits, regarding two-phase flow pattern transitions. *Int. Commun. Heat Mass Transf.*, 1992, **19**(1), 29–39.
3 **Suo, M.** and **Griffith, P.** Two-phase flow in capillary tubes. *J. Basic Eng.*, 1964 **86**, 576–582.

4 **Bretherton, F. P.** The motion of long bubbles in tubes. *J. Fluid Mech.*, 1961, **10**, 166–188.

5 **White, E. T.** and **Beardmore, R. H.** The velocity of rise of single cylindrical air bubbles through liquids contained in vertical tubes. *Chem. Eng. Sci.*, 1962, **17**, 351–361.

6 **Triplett, K. A., Ghiaasiaan, S. M., Abdel-Khalik, S. I., LeMouel, A.,** and **McCord, B. N.** Gas–liquid two-phase flow in microchannels. Part II: void fraction and pressure drop. *Int. J. Multiphase Flow*, 1999, **25**, 395–410.

7 **Chen, L., Tian, Y. S.,** and **Karayiannis, T. G.** The effect of tube diameter on vertical two-phase regimes in small tubes. *Int. J. Heat Mass Transf.*, 2006, **49**, 4220–4230.

8 **Irandoust, S.** and **Andersson, B.** Mass-transfer and liquid-phase reactions in a segmented 2-phase flow monolithic catalyst reactor. *Chem. Eng. Sci.*, 1988, **43**, 1983–1988.

9 **Thulasidas, T. C., Abraham, M. A.,** and **Cerro, R. L.** Dispersion during bubble train flow in capillaries. *Chem. Eng. Sci.*, 1999, **54**, 61–76.

10 **Salman, W., Gavriilidis, A.,** and **Angeli, P.** A model for predicting axial mixing during gas–liquid Taylor flow in microchannels at low Bodenstein numbers. *Chem. Eng. J.*, 2004, 101, 391–396.

11 **Berčič, G.** and **Pintar, A.** The role of gas bubbles and liquid slug lengths on mass transport in the Taylor flow through capillaries. *Chem. Eng. Sci.*, 1997, **52**, 3709–3719.

12 **Taha, T.** and **Cui, Z. F.** Hydrodynamics of slug flow inside capillaries. *Chem. Eng. Sci.*, 2004, **59**, 1181–1190.

13 **Fairbrother. F.** and **Stubbs, A. E.** The bubble-tube method of measurement. *J. Chem. Soc.*, 1935, **1**, 527–529.

14 **Taylor, G. I.** Deposition of a viscous fluid on the wall of a tube. *J. Fluid Mech.*, 1961, **10**, 161–165.

15 **Chen, J. D.** Measuring the film thickness surrounding a bubble inside a capillary. *J. Colloid Interf. Sci.*, 1986, **109**(7), 341–349.

16 **Marchessault, R. N.** and **Mason, S. G.** Flow of entrapped bubbles inside a capillary. *Ind. Eng. Chem.*, 1960, **52**(1), 79-84.

17 **Irandoust, S.** and **Andersson, B.** Liquid film in Taylor flow through a capillary. *Ind. Eng. Chem. Res.*, 1989, **28**, 1684–1688.

18 **Aussilous, P.** and **Quéré, D.** Quick deposition of a fluid on the wall of a tube. *Phys. Fluids*, 2000, **12**(10), 2367–2371.

19 **Goldsmith, H. L.** and **Mason, S. G.** The flow of suspensions through tubes II. Single large bubbles. *J. Colloid Sci.* 1963, **18**, 237–261.

20 **Teletzke, G. F.** *Thin liquid films: molecular theory and hydrodynamic implications*. PhD Thesis, University of Minnesota, 1983.

21 **Schwartz, L. W., Princen, H. M.,** and **Kiss, A. D.** On the motion of bubbles in capillary tubes. *J. Fluid Mech.*, 1986, **172**, 259–275.

22 **Herbolzheimer, E.** The effect of surfactant on the motion of a bubble in a capillary. In Proceedings AIChE Annual Meeting, New York, 15–20 November 1987, paper no. 68j.

23 **Ratulowski, J.** and **Chang, H. C.** Marangoni effects of trace impurities on the motion of long gas bubbles in capillaries. *J. Fluid Mech.*, 1990, **210**, 303–328.

24 **Reinelt, D. A.** and **Saffman, P. G.** The penetration of a finger into a viscous fluid in a channel and tube. *SIAM J. Sci. Stat. Comput.*, 1985, **6**, 542–561.

25 **Shen, E.** and **Udell, K.** A finite element study of low Reynolds number 2-phase flow in cylindrical tubes. *Trans. ASME, J. Appl. Mech.*, 1985, **52**(7), 253–256.

26 **Martinez, M. J.** and **Udell, K.** Boundary integral analysis of the creeping flow of longs bubbles in capillaries. *Trans. ASME, J. Appl. Mech.*, 1989, **56**, 211–217.

27 **Ratulowski, J.** and **Chang, H. C.** Transport of bubbles in capillaries. *Phys. Fluids*, 1989, **A1**, 10, 1642–1655.

28 **Edvinsson, R. K.** and **Irandoust, S.** Finite element analysis of Taylor flow. *AIChE J.*, 1996, **42**(7), 1815–1823.

29 **Giavedoni, M. D.** and **Saita, F. A.** The axisymmetric and plane case of a gas phase steadily displacing a Newtonian liquid – a simultaneous solution to the governing equations. *Phys. Fluids*, 1997, **9**(8), 2420–2428.

30 **Giavedoni, M. D.** and **Saita, F. A.** The rear meniscus of a long bubble steadily displacing a Newtonian liquid in a capillary tube. *Phys. Fluids*, 1999, **11**(4), 786–794.

31 **Heil, M.** Finite Reynolds number effects in the Bretherton problem. *Phys. Fluids*, 2001, **13**(9), 2517–2521.

32 **de Ryck, A.** The effect of weak inertia on the emptying of a tube. *Phys. Fluids*, 2002, **14**(7), 2102–2108.

33 **Thulasidas, T. C., Abraham, M. A.,** and **Cerro, R. L.** Bubble train flow in capillaries of circular and square cross section. *Chem. Eng. Sci.*, 1995, **50**(7), 183–199.

34 **Wallis, G. B.** *One-dimensional two-phase flow*, 1969 (McGraw-Hill Book Company, New York).

35 **Cox, B. G.** An experimental investigation of the streamlines in viscous fluid expelled from a tube. *J. Fluid Mech.*, 1964, **20**, 193–200.

36 **Laborie, C., Cabassud, L., Durand-Bourlier,** and **Laine, J. M.** Characterisation of gas–liquid two-phase flow inside capillaries. *Chem. Eng. Sci.*, 1999, **54**, 5723–5735.

37 **Liu, H., Vandu, C. O.,** and **Krishna, R.** Hydrodynamics of Taylor flow in vertical capillaries: flow regimes, bubble rise velocity, liquid slug length and pressure drop. *Ind. Eng. Chem. Res.*, 2005, **44**, 4884–4897.

38 **Akbar, M. K.** and **Ghiaasiaan, S. M.** Simulation of Taylor flow in capillaries based on the volume-of-fluid technique. *Ind. Eng. Chem. Res.*, 2006, **45**, 5396–5403.

39 **Kreutzer, M. T.** *Hydrodynamics of Taylor flow in capillaries and monolith reactors*. PhD Thesis, Technical University of Delft (TUD), 2003.

40 **Kreutzer, M. T., van der Eijnden, M. G., Kapteijn, F., Moulijn, J. A.,** and **Heiszwolf, J. J.** The pressure drop experiments to determine slug lengths in multiphase monoliths. *Catal. Today*, 2005, **105**, 667–672.

41 **Qian, D.** and **Lawal, A.** Numerical study on gas and liquid slugs for Taylor flow in a T-junction microchannel. *Chem. Eng. Sci.*, 2006, **61**, 7609–7625.

42 **Amador, C., Salman, W., Sanguanpiyapan, S., Gavriilidis, A.,** and **Angeli, P.** Effect of gas/liquid inlet conditions on slug length in Taylor flow. In Proceedings of the 5th International Conference on Multiphase Flow (CD-ROM), Japan, 30 May–4 June 2004.

43 **Salman, W., Gavriilidis, A.,** and **Angeli, P.** On the formation of Taylor bubbles in small tubes. *Chem. Eng. Sci.*, 2006, **61**, 6653–6666.

44 Westborg, H. and **Hassager, O.** Creeping motion of long bubbles and drops in capillary tubes. *J. Colloid Interf. Sci.*, 1989, **133**(1), 135–147.

45 Thulasidas, T. C., Abraham, M. A., and **Cerro, R. L.** Flow patterns in liquid slugs during bubble-train flow inside capillaries. *Chem. Eng. Sci.*, 1997, **52**(12), 2947–2962.

46 Kreutzer, M. T., Kapteijn, F., Moulijn, J. A., Kleijn, C. R., and **Heiszwolf, J. J.** Inertial and interfacial effects on pressure drop of Taylor flow in capillaries. *AIChE J.*, 2005, **105**, 667–672.

47 Kolb, W. B. and **Cerro, R. L.** Coating the inside of a capillary of square cross section. *Chem. Eng. Sci.*, 1991, **46**(9), 2181–2195.

48 Kolb, W. B. and **Cerro, R. L.** Film flow in the space between a circular bubble and a square tube. *J. Colloid Interf. Sci.*, 1993, **159**, 302–311.

49 Kolb, W. B. and **Cerro, R. L.** The motion of long bubbles in tubes of square cross section. *Phys. Fluids*, 1993, **5**(7), 1549–1557.

50 Taha, T. and **Cui, Z. F.** CFD modelling of slug flow inside square capillaries. *Chem. Eng. Sci.*, 2006, **61**, 665–675.

51 Hazel, A. L. and **Heil, M.** The steady propagation of a semi-infinite bubble into a tube of elliptical or rectangular cross section. *J. Fluid Mech.*, 2002, **470**, 91–114.

52 Kreutzer, M. T., Kapteijn, F., Moulijn, J. A., Kleijn, C. R., and **Heiszwolf, J. J.** Multiphase monolith reactors: chemical reaction engineering of segmented flow in microchannels. *Chem. Eng. Sci.*, 2005, **60**, 5895–5916.

53 Fries, D. M., Trachsel, F., and **von Rohr, P. R.** Optical characterization of phase distribution in gas–liquid Taylor flow in rectangular microfluidic channels. In Proceedings of the 5th International Conference on Multiphase Flow (ICMF'04), Yokohama, Japan, 30 May–4 June 2007, paper no. S7_Thu_A_47.

54 Cubaud, T., Ulmanella, U., and **Ho, C. M.** Two-phase flow in microchannels with surface modifications. In Proceedings of the 5th International Conference on Multiphase Flow (ICMF'04), Yokohama, Japan, 30 May–4 June 2004, paper no. PL2.

55 Tsoligkas, A. N., Simmons, M. J. H., and **Wood, J.** Influence of orientation upon the hydrodynamics of gas–liquid flow for square channels in monolith supports. *Chem. Eng. Sci.*, 2007, **62**, 4365–4378.

56 Heiszwolf, J. J., Kreutzer, M. T., van der Eijnden, M. G., Kapteijn, F., and **Moulijn, J. A.** Gas–liquid mass transfer of aqueous Taylor flow in monoliths. *Catal. Today*, 2001, **69**(1–4), 51–55.

57 Garstecki, P., Fuerstman, M. J., Stone, H. A., and **Whitesides, G. M.** Formation of droplets and bubbles in a microfluidic T-junction – scaling and mechanism of break-up. *Lab on a Chip*, 2006, **6**, 437–446.

58 Cubaud, T., Tatineni, M., Zhiong, X., and **Ho, C. M.** Bubble dispenser in microfluidic device. *Phys. Rev.*, 2005, **72**, 037302.

59 Xiong, R., Bai, M., and **Chung, J. N.** Formation of bubbles in a simple co-flowing micro-channel. *J. Micromech. Microeng.*, 2007, **17**, 1002–1011.

APPENDIX

Notation

Bo	Bond number (–)
C	coefficient in equation (8) (–)
Ca	capillary number (–)
C_f	constant in the friction factor-Reynolds number relation (see equation (27) (–)
C_o	coefficient in equation (14) (–)
d	channel diameter (m)
d_b	bubble diameter in diagonal direction in a square channel, see equation (29) (m)
$d_{channel}$	square channel side length, see equation (29) (m)
$E\ddot{o}$	Eötvos number, equivalent to Bo number (–)
f	Fanning friction factor (–)
F_E	friction factor defined by equation (27) (–)
Fr	Froude number (–)
g	acceleration of gravity (m/s^2)
h_0	dimensionless film thickness (–)
L	channel length (m)
L_B	bubble length (m)
L_S	slug length (m)
L_{UC}	unit cell length (m)
m	relative bubble velocity defined by equation (10) (–)
N_f	fluid property number (–)
ΔP	pressure difference (Pa)
Q	volumetric flowrate (m^3/s)
r	channel radius (m)
r^0	centre of toroidal vortex in liquid slug (m)
r^1	radial position of streamline that separates the circulating vortex in the slug from the liquid film attached to the wall (m)
Re	Reynolds number (–)
S	slip ratio, ratio of gas-to-liquid velocity in the channel (–)
U_b	bubble velocity (m/s)
Ue	gravity equivalent velocity defined in equation (27) (m/s)
U_E	two-phase velocity defined in equation (27) (m/s)
U_g	gas superficial velocity (m/s)
U_l	liquid superficial velocity (m/s)
U_{ls}	average slug velocity (m/s)
U_m	two-phase mixture velocity, $U_g + U_l$ (m/s)
U_o	bubble rise velocity in a stagnant liquid (m/s)
w	main channel width in equation (31) (m)
We	Weber number (–)

δ	film thickness (m)
ε	volume fraction
μ	viscosity (Pa s)
ρ	density (kg/m^3)
σ	surface tension (N/m)
ψ	ratio of bubble to mean flow velocity

Subscripts

b	bubble
g	gas
l	liquid
S	slug
TP	two-phase